Journal of Korea TAPPI
Vol. 31. No. 5, 1999
Printed in Korea

Distortion and Dilatation in the Tensile Failure of Paper

Jong-Moon Park† and James L. Thorpe*

ABSTRACT

Yield and fracture are separated in the tensile failure of paper. Failure in the machine direction of photocopy paper is contrasted with failure in the cross-machine direction. The ratios of distortion (shape change) to dilatation (volume change) for individual elements at yield and fracture are described.

The ratios of distortion to dilatation are measured and compared to predicted values of the strain energy density theory. To evaluate the effect of the angle from the principal material direction on the strain energy density factor, samples are prepared from machine direction to cross-machine direction in 15 degree intervals. The strain energy density of individual elements are obtained by the integration of stress from finite element analysis with elastic plus plastic strain measured of individual elements over the complete loading history.

The measured ratios of distortion to dilatation at yield agree with the predicted ratios by the strain energy density theory. Poisson's ratio and the angle from the principal material direction have a great effect on the ratio of distortion to dilatation in paper. During the yield condition, distortion prevails over dilatation. At fracture, dilatation is at a maximum.

1. Introduction

Yield and fracture are different quantitatively in the machine direction and cross-machine direction for most papers. In this paper the rations of distortion (shape change) to dilatation (volume change) of local elements in mode I tensile analysis are examined experimentally. A theory is developed to compare the yield and fracture with the experimental results.

Yield can be defined as a failure by excessive distortion associated with a shape change that leads to permanent deformation. Fracture can be defined as a failure by excessive dilatation associated with a volume change that results in physical separation of a material. Yield and fracture are quite different in a mechanism in which energy is absorbed. A completely brittle material has only fracture or dilatation as a failure mechanism. A completely ductile material has only yield or distortion as a failure mechanism. Usually a material like paper exhibits yield and fracture simultaneously as a failure mechanisms.

In most service conditions, paper is under a mixed mode loading of not only tension but also shear. As a composite of randomly distributed fibers, the tensile failure mecha-

• This research had been supported by Empire State Paper Research Institute, USA.
• School of Forest Resources, Chungbuk Nat'l Univ., Cheongju 361-763, Korea.
* College of Environmental Science & Forestry, State Univ. of New York, Syracuse, NY 13210, USA.
† Corresponding author: e-mail: jmpark@cbucc.chungbuk.ac.kr

nisms include breakage of fibers as well as the bonding areas between fibers. On a microscopic scale, the fibers and bonds can be characterized by a micro-mechanics model in which the paper is regarded as a non-continuum material. However on a macroscopic scale, paper can be regarded as a continuum. The validity of the continuum approximation for paper is tested here with a comparison of the initial angle of fracture propagation reported in previous work.[1)]

Micromechanics model theories, that have followed the Cox theory,[2)] have provided a great deal of insight into paper strength, but they have variables that are difficult or impossible to quantify with current knowledge and experimental techniques. The classical fracture mechanics of Griffith's strain energy releases rate theory[3, 4)] can be applied to elastic material in pure mode I tensile loading. The strain energy density theory[5-7)] can be applied for elastic plastic material, with or without flaws, under mixed mode loading conditions. For tough paper the strain energy density theory has advantages over Griffith's theory as tensile yield and fracture can be explained.

1. 1 Dilatation and distortion

In this analysis the area between the initial edge cracks of each test specimen is subdivided into imaginary elements that can be examined for stress, strain, and strain energy density.

Material can absorb energy in two basic ways, by dilatation, i.e., a change in volume, and/or distortion, i.e., a change in shape. Fig. 1 shows that a distortion of material with a crack is associated with yielding at the sides of a crack under symmetric loading. Dilatation or volume change of a material tends to be associated with the creation of free surface or fracture that occurs along the line of the initial crack.

The classic von Mises' theory for failure only accounts for yield by distortion, S_d, while dilatation, S_v, is neglected[7)]. The dilatation energy in the mode I tensile failure of paper can not be ignored because the magnitude of the dilatation energy is comparable to the distortion energy.

The assumption of a linear relationship between stress and strain allows the separation of the strain energy density function, dw/dv, into its distortional, $(d_w/d_v)_d$, and dilatational components, $(d_w/d_v)_v$.

$$(dw/dv)=(dw/dv)_d+(dw/dv)_v \qquad [1]$$

Stress in paper can be assumed to be plane stress. The rectangular stress components σ_x, σ_y, and τ_{xy} are shown in Fig. 2. Stress components σ_z, τ_{xz}, and τ_{yz} are taken to be zero. The Cartesian coordinate axis x is in a horizontal direction which is the same as the direction of the initial crack. The Cartesian coordinate axis y is in a vertical direction which is same as the direction of the tensile loading. Two principal stresses can be calculated from the rectangular stresses. The large principal stress is denoted as σ_1 and the small principal stress is denoted as σ_2.

Based on the total energy theory[8, 9)] and the distortion energy theory,[10-12)] the strain energy density function, dw/dv, can be expressed by rectangular stress components or principal stress components for a plane stress case.

$$(dw/dv)_d=\{(7-\kappa)/(12E)(\sigma_x^2-\sigma_x\sigma_y+\sigma_y^2+3\tau_{xy}^2)$$
$$(dw/dv)_v=\{(\kappa-1)/(12E)(\sigma_x+\sigma_y)^2$$
$$(dw/dv)_d=\{(7-\kappa)/(12E)\ (\sigma_1^2-\sigma_1\sigma_2+\sigma_2^2)$$
$$(dw/dv)_v=\{(\kappa-1)/(12E)(\sigma_1+\sigma_2)^2 \qquad [2]$$

where the elastic constant κ is $(3-\gamma)/(1+\gamma)$ and γ is the Poisson's ratio.

The strain energy density factor S is

defined and known as follows :

$$S= r(dw/dv)$$
$$S=a_{11}k_1^2+2a_{12}\,k_1\,k_2+a_{22}k_2^2 \qquad [3]$$

where r is the distance of an element from the crack tip.

The stress intensity factors k_1 and k_2 correspond to the mode I and mode II loading, respectively. The coefficients a_{ij} ; i, j = 1, 2, are as follows :

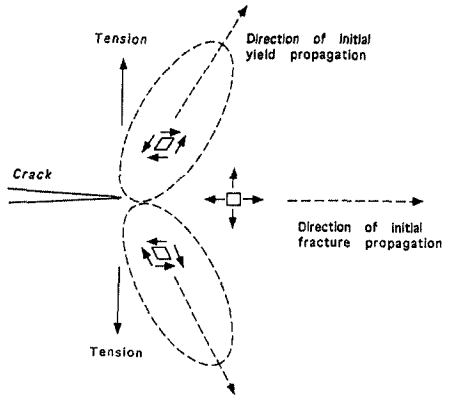

Fig. 1. Yield and fracture of elements in front of a crack tip where *dw/dv* corresponds to the area under the stress-strain curve.

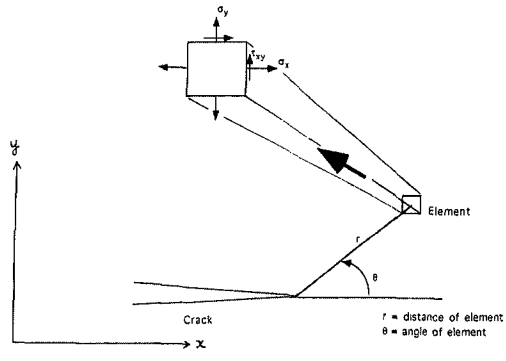

Fig. 2. Rectangular stress components of an element.

$$a_{11}= \frac{1}{16\mu}[(1+\cos\theta)(\kappa-\cos\theta)]$$

$$a_{12}= \frac{1}{16\mu}\sin\theta[2\cos\theta-(\kappa-1)]$$

$$a_{22}= \frac{1}{16\mu}[(\kappa-1)(1-\cos\theta)+(1+\cos\theta)(3\cos\theta-1)] \qquad [4]$$

where μ is shear modulus and θ is the angle of an element from the crack tip.

The strain energy density factor S can also be separated into two parts, namely distortion part, S_d, and dilatation part, S_v.

$$S=S_d+S_v \qquad [5]$$

where ;

$$S_d=c_{11}k_1^2+2c_{12}\,k_1\,k_2+c_{22}k_2^2$$
$$S_v=b_{11}k_1^2+2b_{12}\,k_1\,k_2+b_{22}k_2^2 \qquad [6]$$

The coefficients b_{ij} and c_{ij}, i, j = 1, 2, are as follows;

$$b_{11}=\{1/(12\mu)\}\{(\kappa-1)/2\}\{(7-\kappa)/4\}(1+\cos\theta)$$
$$b_{12}=\{1/(12\mu)\}\{(\kappa-1)/2\}\{(7-\kappa)/4\}(\sin\theta)$$
$$b_{22}=\{1/(12\mu)\}\{(\kappa-1)/2\}\{(7-\kappa)/4\}(1-\cos\theta)$$
$$c_{11}=\{1/(16\mu)\}(1+\cos\theta)[\{(\kappa-1)^2/6\}+1-\cos\theta]$$
$$c_{12}=\{1/(16\mu)\}(\sin\theta)[2\cos\theta-\{(\kappa-1)^2/6\}]$$
$$c_{22}=\{1/(24\mu)\}[\{(\kappa-1)^2/4\}(1+\cos\theta)+4-3\sin^2\theta] \qquad [7]$$

To determine the relative effects of dilatation and distortion at the onset of yield and fracture, the relative ratio of S_d and S_v should be analyzed at the location of each element of yield and fracture.

Three loading cases can be considered, (a) uniaxial tension, (b) pure shear, and (c) mixed mode. Procedures to obtain the ratio of distortion to dilatation in yield and fracture are the same for all three cases. Uniaxial tension is more common than the other cases, so the uniaxial condition will be discussed with experimental results in this paper.

1. 2 Uniaxial tension

Under uniaxial tension a sharp double-edge notched crack propagates normal to the loading direction along the line of the original crack. The strain energy density theory states that at fracture the strain energy density factor S has a relative minimum, S_{min}, with the condition $\partial S/\partial\theta = 0$. The values S_{min}, S_d, S_v, and the ratio, S_d/S_v, can be obtained when the direction of original crack is normal to the uniaxial tension.

$$S=\{1/(16\mu)\}(\kappa-\cos\theta)(1+\cos\theta)k_1^2 \quad [8]$$
$$S_{min}=\{(\kappa-1)/(8\mu)\}k_1^2 \quad [9]$$

When the initial crack starts to propagate on tensile loading S_{min} approaches the critical value of the strain energy density factor, S_c, which represents the fracture toughness of the material and the above equation becomes

$$k_1^2=\sigma^2 a$$
$$S_c=\{(\kappa-1)(7-\kappa)/(16E)\}\sigma_c^2 a \quad [10]$$

where σ is remote stress, σ_c is critical remote stress at the initial crack propagation, and represents crack length.

From equation [6], S_{min} can be decomposed into two parts and S_d and S_v can be calculated.

$$S_d=\{(\kappa-1)^2/(48\mu)\sigma_c^2 a$$
$$S_v=\{(\kappa-1)(7-\kappa)/(48\mu)\sigma_c^2 a \quad [11]$$

Therefore,

$$S_d/S_v=(\kappa-1)/(7-\kappa) \quad [12]$$

At yield the strain energy density factor S reaches the relative maximum, S_{max}. With the same procedure, the relative maximum of S and its ratio can be calculated by using the strain energy density theory's conditions.

$$S_{max}=\{(1+\kappa)^2/64\mu\}k_1^2 \quad [13]$$
$$S_d=\{(1+\kappa)(10-5\kappa+\kappa^2)/(96\mu)\}\sigma_c^2 a$$
$$S_v=\{(\kappa-1)(7-\kappa)(1+\kappa)/(384\mu)\}\sigma_c^2 a \quad [14]$$

Therefore S_{max} gives the ratio of dilatation and distortion. The ratio S_d/S_v at yield becomes

$$S_d/S_v=4(10-5\kappa+\kappa^2)/\{(\kappa-1)(7-\kappa)\} \quad [15]$$

2. Materials and Methods

Photocopy paper was used in this study. Double-edge notched, dog-bone shaped specimens were used in the testing as described in previous work.[13] The principal material direction of each specimen was determined by the ultrasonic technique.[14] The angle of incline, α, from the principal material direction was incremented by 0, 15, 30, 45, 60, and 75° as shown in Fig. 3. When the angle of incline, α, from the principal material direction of specimen is 0°, the specimen is a machine direction sample. When the incline angle is 75°, the specimen is approaching a cross-machine direction sample.

The rate of elongation on the Instron 4204 was 10 mm/min. Strains were analyzed by the linear image strain analysis (LISA)[15] and stresses were calculated with finite element analysis.[16]

The observation area of LISA was 35.4 mm wide and 38.9 mm high. That area was broken into 280 strain observation elements, a 14 by 20 grid, each 2.53 mm wide by 1.95 mm high. The finite element analysis grid for calculating stresses in the observation area was identical in size and the number of elements.

A series of strain profiles were prepared using LISA to observe the effect of incline

angle, α, from the principal material direction on the strain. The strain energy density of individual elements is obtained by the integration of stress with elastic plus plastic strain of individual elements over the complete loading history as demonstrated in previous work.[17] The strain energy density factor of each element is obtained by multiplying the distance, r, from the crack tip and the strain energy density of the element.

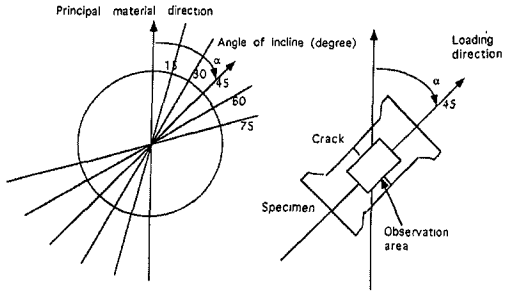

Fig. 3. The angle of incline, α, of double edge-notched fracture sample.

To compare the measured and predicted ratios of distortion to dilatation at yield and fracture, the measured ratios are obtained from the rectangular stress components generated by the finite element analysis system ANSYS and equation [2]. The predicted ratios of distortion to dilatation at yield are obtained by using equation [15] and the predicted ratios at fracture are obtained by using equation [12]. When the ratio of distortion to dilatation is greater than 1, the distortion part of the strain energy density factor, S_d is greater than the dilatation part, S_v. Physically it means more strain energy is absorbed by the shape change than by the volume change.

3. Results and Discussion

3. 1 Results

3. 1. 1 Strain profiles and strain energy density factor profiles

In Fig. 4, the near-failure strain profiles of photocopy paper are shown for the six separate test at an increasing angle of orientation from the principal material direction in 15° increments from 0 to 75°. The areas over 2.0% strain are shaded lightly and over 3.0% strain are given a dark shading. Load is expressed in kilograms and the angle of incline, α, from the principal material direction in degrees as shown above each figure. Failure load and failure strain are shown under each figure.

Fig. 4(a), at α=0°, is the near-failure strain profile at 13.3 kg_f load (99.9% of failure load) and at 0.62% strain (95.4% of failure strain). Areas over 1.0% strain show up in front of the crack tip and at bottom of the observation area. Most of the observation area is over 0.5% strain. Fig. 4(b), at α= 15°, is the near-failure strain profile at 12.4 kg_f (97.9% of failure load) and at 0.69% strain (93.2% of failure strain). Areas above 1.0% strain between the two edge cracks are connected by an area approaching 1.0% strain. Fig. 4(c), at α= 30°, is the near-failure strain profile at 9.4 kg_f (92.7% of failure load) and at 0.60% strain (87.0% of failure strain). Areas greater than 3.0% strain appear in front of the left crack tip as well as the top right of the observation area. Strain areas over 1.0% are connected in the top of the observation area. Fig. 4(d), at α= 45°, is the near-failure strain profile at 9.3 kg_f (98.1% of failure load) and at 0.73% strain (93.6% of failure strain). Most of the observation area is overstrain 1.0% strain. An area greater than 1.5% strain is enlarged beyond the area shown in Fig. 4(c). Fig. 4(e), at α= 60°, is the near-failure strain profile at 8.2 kg_f (97.7% of

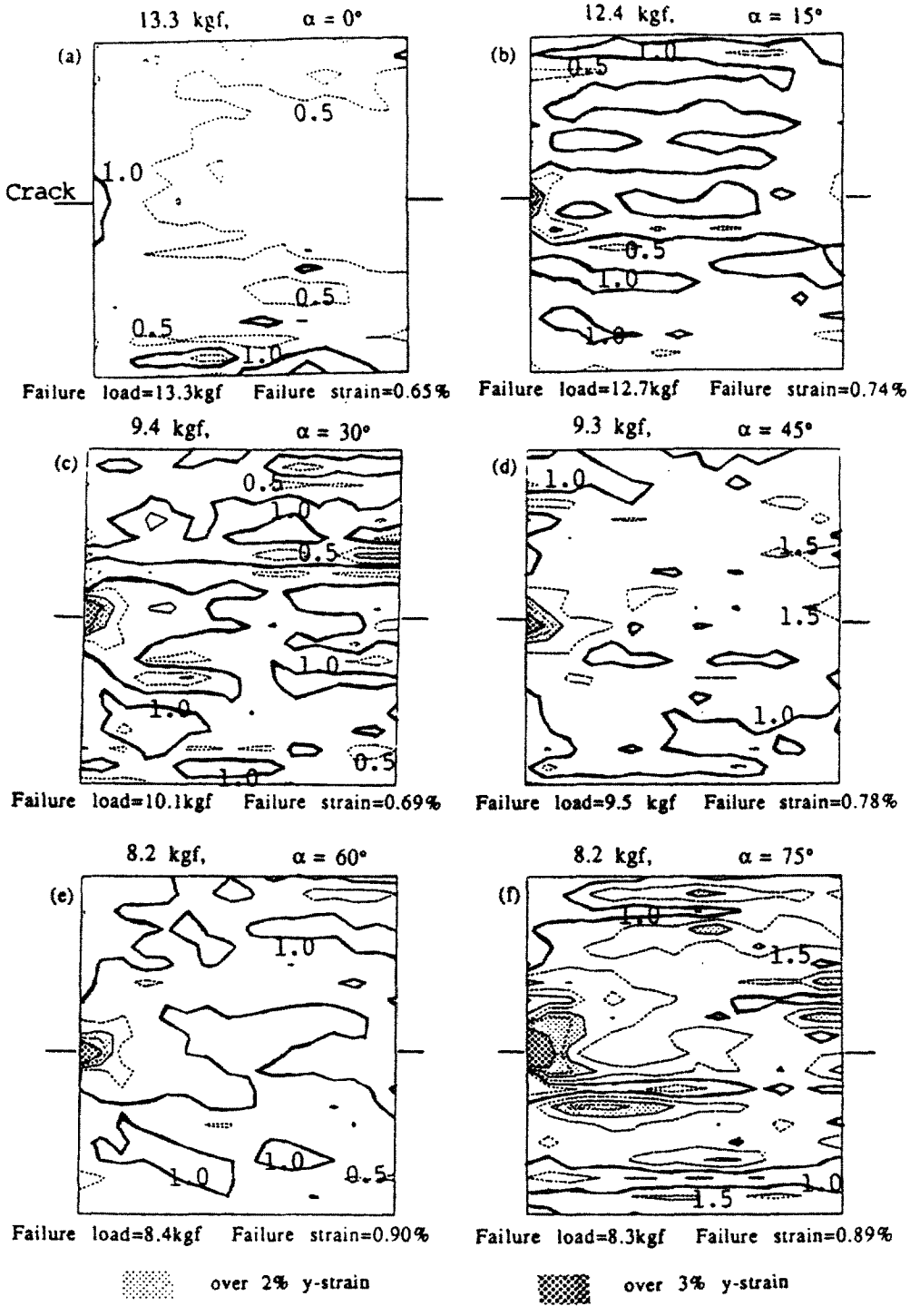

Fig. 4. Near-failure strain profiles of photocopy paper whose loading direction has been progressively increased from the principal material axis.

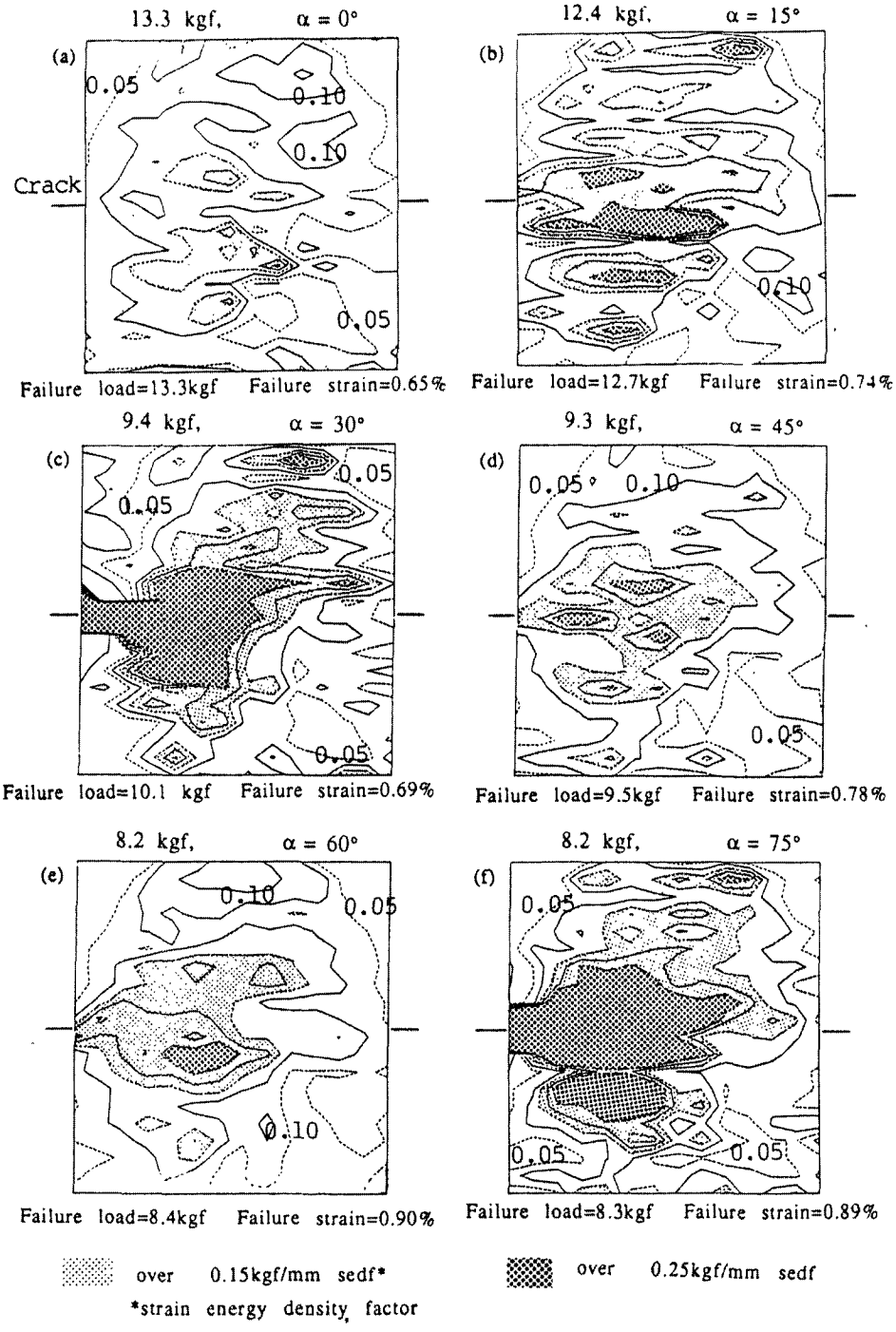

Fig. 5. Near-failure strain energy density factor profiles of photocopy paper whose loading direction has been progressively increased from the principal material axis.

failure load) and at 0.84% strain (93.3 of failure strain). Most of the observation area is over 1.0% strain. Fig. 4(f), at α= 75°, is the near-failure strain profile at 8.2 kg_f (98.1% of failure load) and at 0.81% strain (91.0% of failure strain). Areas above 2.0% are observed in front of the crack tip and along the lower left side of the observation area and several isolated locations. There is a progression of 3.0% strain areas that increases from Fig. 4(a) through 4(f).

In Fig. 5, the near-failure strain energy density factor profiles of photocopy paper are shown at increasing angular orientation from the principal material direction. Areas over 0.15 kg_f/mm are shaded lightly and areas over 0.25 kgf/mm are in a darker shading. Conditions of load are expressed in kilograms and the angle of incline, α, from the principal material direction in degrees as shown above each figure. Failure load and failure strain are shown under each figure.

Fig. 5(a), at α = 0°, is the near-failure strain energy density factor profile at 13.3 kg_f (99.9% of failure load) and at 0.62% strain (95.4% of failure strain). Areas of the strain energy density factor over 0.15 kg_f/mm appear in several isolated locations at the center of the observation area. Fig. 5(b), at α= 15°, is the near-failure strain energy density factor profile at 12.4 kg_f (97.9% of failure load) and at 0.69% strain (93.2 of failure strain). Areas over 0.25 kg_f/mm appear at several isolated locations are observed. Wide areas over 0.15 kg_f/mm are scattered throughout the observation area. Fig. 5(c), at = 300, is the near-failure strain energy density factor profile at 9.4 kg_f (92.7% of failure load) and at 0.60% strain (87% of failure strain). Areas over 0.25 kg_f/mm are concentrated in front of the crack tip. Fig. 5(d), at α= 45°, is the near-failure strain energy density factor profile at 9.3 kg_f (98.1% of failure load) and at 0.73% strain (93.6% of failure strain). Several areas over 0.25 kg_f/mm are observed at isolated locations in front of the left side crack. Broad areas over 0.15 kg_f/mm are shown at the center of the observation area. Fig. 5(e), has a wide area over 0.15 kg_f/mm at the center of the observation area that is connected to the left side crack tip. Fig. 5(f), at α= 75°, is the near-failure strain energy density factor profile at 8.2 kg_f load (98.1% of failure load) and at 0.81% strain (91.0% of failure strain). Areas over 0.25 kg_f/mm are very wide in front of the left side crack tip.

3. 2 Discussion

The experimental strain profiles are used to determine both yield and fracture within the tensile specimens. When the strain value of an area is greater that 125% of the total failure strain without fracture, the failure mode of the area is assumed to be due to yield. When the strain value of an area is greater that 125% of the total failure strain and fracture is apparent within that area after tensile failure, the failure is assumed to be by fracture. The strain energy density factor profiles display the distribution of the strain energy density factor throughout the observation area. The strain energy density factor profiles are the product of the measured strains and the stresses calculated from the finite element analysis. The theory developed has shown that the strain energy density factor can be separated into distortion and dilatation. The ratio of distortion to the dilatation can be predicted at yield and fracture by the strain energy density theory. The ratios of distortion to dilatation indicate the relative amount of strain energy absorption by shape change and volume change during tensile loading.

3. 2. 1 Strain profiles and strain energy density factor profiles

Fig. 4 presents the near-failure strain profiles of six samples of photocopy paper with the angle from the principal material direction increased in 15° increments from 0 to 75°. There is a progressive increase in the strain area above 2.0% and 3.0% as the angle from the principal material axis is increased. Areas over 2.0% strain, in the light shading, appear more concentrated at the crack tip when the angle of incline from the principal material direction is 15° than when the angle of incline is 75°. When the angle of incline from the principal material axis is small, high strain regions do not propagate. When the angle of incline from the principal material direction increases toward the cross-machine direction, the areas over 2.0% increases.

Fig. 5 presents the near-failure strain energy density factor profiles for photocopy paper with progressively increased angles away from the principal material direction. The product of the local stresses and strains and the distance from crack tip reflect the energy absorption in the six specimens. In Fig. 5(a), at $\alpha = 0°$, few areas reach 0.15 kg_f/mm of the strain energy density factor prior to failure. Therefore little strain energy is absorbed prior to failure. When the incline angle is low or near the machine direction, individual fibers are more likely to take up the external tensile load than fiber bonding. Individual fibers are more brittle and elastic in nature than the fiber-to-fiber bonds which appear to be quite plastic, so the amount of absorbed energy is small. In Fig. 5(f), at $\alpha = 75°$, fiber bonding is more likely to take up the external tensile load than individual fibers. Fiber bonding is more ductile and likely to deform in shear to absorb a larger amount of applied energy. Therefore, as the incline angle, α, from the principal material direction increases incrementally from 0 to 75°, the areas of strain energy density factor over 0.25 kg_f/mm generally increase.

As shown in Fig. 5(a)-(f), the strain energy density factor reaches or exceeds 0.15 kg_f/mm just prior to failure. This critical or limiting value of the strain energy density factor may be considered as a characteristic material parameter for this specific paper and used to predict failure.

Generally speaking, the propagation direction for the strain energy density factor profiles of Fig. 5 are diagonally upward and downward, and straight ahead of the original crack. The strain energy density factor profile is a good indicator of the directions of yield and fracture for paper before failure.

3. 2. 2 Ratios of distortion to dilatation of the strain energy density factor at yield and fracture

When the Poisson's ratio of a specimen is known, the ratios of distortion to dilatation can be predicted. At yield, the predicted ratio of distortion to dilatation is obtained by using equation [15]. At fracture, the predicted ratio of distortion to dilatation is obtained by using equation [12].

The measured ratios of distortion to dilatation are obtained by substituting the rectangular stress components from the finite element analysis into equation [2]. The strain energy density factor ratio of distortion to dilatation, S_d/S_v, for each element is same as the strain energy density ratio of distortion to dilatation, $(d_w/d_v)_d/(d_w/d_v)_v$, because the distance, r, from crack tip is same. It can be shown by equation as follows;

$$\frac{S_d}{S_v} = \frac{(d_w/d_v)_d \times r}{(d_w/d_v)_v \times r} = \frac{(d_w/d_v)_d}{(d_w/d_v)_v}$$

Therefore, the ratio of distortion to dilatation, S_d/S_v, can be obtained directly by substituting the rectangular stress components from the finite element analysis into equation [2].

Examples of the measured ratios of distortion to dilatation are obtained for seven elements, as shown in Fig. 6. The most feasible locations of yield and fracture are near the crack tip. The locations of the seven elements are described by the distance r and angle θ from the crack tip in Table 1. The principal stress ratio σ_1/σ_2 is used to describe the stress conditions of an element. The principal stress components σ_1 and σ_2 and their ratios σ_1/σ_2 can be obtained from the rectangular stress components of each element generated by the finite element analysis. The measured ratios of distortion to dilatation are included. When the principal stress ratio σ_1/σ_2 is one, dilatation is at a maximum. When the principal stress ratio σ_1/σ_2 increases beyond one, distortion prevails over dilatation.

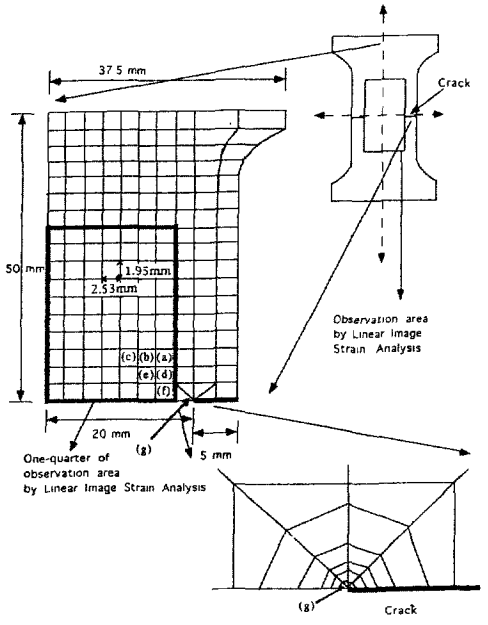

Fig. 6. Location of elements (a)-(h) in one-quarter of the observation area.

The failure mode, yield or fracture, can be decided according to the assumption; when the strain value of an area is greater that 125% of the total sample failure strain and fracture is not observed after tensile failure test, the failure mode of the area is yield. When the strain value of an area is greater than 125% of the total sample failure strain and fracture is observed after tensile failure test, the failure mode of the area can be thought of as fracture. The state of elements (a)-(d) is yield because they have reached 125% of failure strain of the whole specimen but fracture did not propagate through the region. The state of elements (e)-(f) is between yield and fracture. The state of element (g) is fracture because fracture can be observed through the element after tensile failure and the strain value is larger than 125% of the failure strain.

The stress conditions in plane stress can be represented by three rectangular stress components σ_x, σ_y, and τ_{xy}. Two perpendicular directions can be found for which the shear stress is zero. These directions are called the principal directions and the corresponding normal stresses are called the principal stresses. By convention the larger of the two principal stresses is expressed as the principal stress σ_1 and smaller of the principal stresses is expressed as the principal stress σ_2.

When the principal stress ratio σ_1/σ_2 is one, the rectangular stress components $\sigma_x = \sigma_y$ and $\tau_{xy} = 0$. The volume change is at the maximum.

When the principal stress ratio σ_1/σ_2 increases beyond one, the magnitude of σ_1 surpasses that of σ_2. It is known that the maximum shear stress of an element is pro-

Table 1. Failure modes of elements and the measured ratio of distortion to dilatation

Element	Distance r (mm)	Angle θ (degrees)	σ_1/σ_2 (unitless)	S_d/S_v (unitless)	Failure mode
(a)	6.0	54	73.461	4.39	Yield
(b)	7.8	39	10.462	3.48	Yield
(c)	8.6	29	7.175	3.10	Yield
(d)	4.6	39	7.218	3.10	Yield
(e)	6.1	26	5.145	2.70	Yield / Fracture
(f)	3.6	15	2.929	1.97	Yield / Fracture
(g)	0.0	0	1.651	1.35	Fracture

portional to the difference of σ_1 and σ_2. As the principal stress ratio σ_1/σ_2 increases from one, the shear stress increases, along with the distortion effect and a shape change prevails over volume change. When the principal stress ratio σ_1/σ_2 reaches a critical ratio of distortion to dilatation yielding occurs.

The predicted and measured ratios of distortion to dilatation are compared in Fig. 7. On the abscissa the ratios of principal stresses σ_1/σ_2 are presented. On the ordinate, the ratios of distortion to dilatation are presented. Fig. 7 also shows that the predicted ratios of distortion to dilatation, S_d/S_v, increases as the principal ratio σ_1/σ_2 increases from one. The minimum of the predicted ratio, S_d/S_v, is reached at the fracture condition at the ratio σ_1/σ_2 is close to 1.0. The measured ratios, S_d/S_v, for points a-f, with a Poisson's ratio of 0.3 are plotted on Fig. 7.

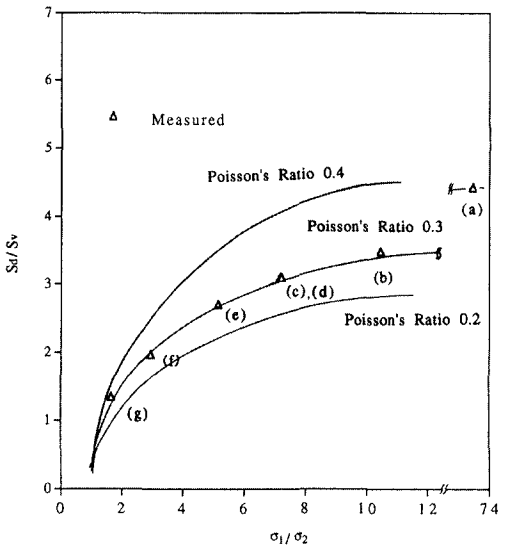

Fig. 7. Ratio of the distortion to dilatation parts of the strain energy density factor for a state of plane stress.

In the yield condition, the predicted ratios of distortion to dilatation increases as the Poisson's ratio increases. At the same principal stress ratio of σ_1/σ_2, the predicted ratio of distortion to dilatation is a function of the Poisson's ratio, γ. The measured ratios of distortion to dilatation of the strain energy density factor given in equation [2] are close to the predicted values of the strain energy density theory given in equation [15]. For example, when the Poisson's ratio is 0.3, the predicted ratio of distortion to dilatation, S_d/S_v, at yield 2.96, whereas the measured ratio is 3.10.

The ratio of distortion to dilatation at fracture is small, so the differences of the predicted ratios at fracture of the Poisson's ratio from 0.2 to 0.4 are not significant as shown in Fig. 7. At fracture, the measured ratios of the distortion to dilatation are not close to the predicted ratios. The predicted ratio of the distortion to dilatation S_d/S_v, at fracture is 0.22 and the measured ratio is 1.35 for photocopy paper of Poisson's ratio 0.3. The strain energy density theory assumes fracture occurs under a linear relationship of

stress and strain, the predicted ratio of distortion to dilatation of the strain energy density factor at fracture could be cloder to the measured ratio.

As the incline angle from the principal material direction increases toward the cross-machine direction, the ratio of distortion to dilatation, S_d/S_v, increases. As the specimen goes from the machine direction to the cross-machine direction, the propagation distance of yield zone also increases and the stress ratio σ_1/σ_2 increases to reach a higher predicted ratio of S_d/S_v. Therefore, the propagation distance of the yield zone should be considered as well as the Poisson's ratio when the predicted ratio of distortion to dilatation is analyzed as the specimen goes from the machine direction to the cross-machine direction.

Under yield conditions, distortion prevails over dilatation. At the fracture condition, dilatation is at a maximum. In an element under yield, like elements (a)-(d), near the crack tip, the ratio of distortion to dilatation, S_d/S_v, is larger than 3.10. In an element in the near fracture state, like element (g), near the crack tip, the stress ratio σ_1/σ_2 is near 1 and the ratio of distortion to dilatation, S_d/S_v, approaches a minimum and dilatation is at a maximum.

The size of yield and fracture zones are related to their ability to absorb the strain energy applied by external tensile loading. The yield zone is a broad area, where the strain energy can be absorbed efficiently. The fracture zone is narrow as a line, where the strain energy is absorbed inefficiently and the stress is concentrated. The yield zone is regarded as the region of the high resistance to fracture propagation. By absorbing the strain energy through efficient distortion and plastic deformation. The yield zone can share the strain energy with surrounding regions. Less strain energy can be absorbed by dilatation at the fracture zone before failure. The fracture zone is regarded as weak zone or the region of the low resistance to fracture propagation. Applied strain energy is concentrated in narrow region so the fracture zone is rather narrow.

4. Conclusions

The strain energy density theory can be applied to analyze the ratio of distortion to dilatation in the yield and fracture of paper. The measured ratio of distortion to dilatation at yield agrees well with the predicted ratio by the strain energy density theory. Poisson's ratio has a great effect on the ratio of distortion to dilatation in each paper grade. The angle from the principal material direction should be considered in terms of the yield zone propagation as well as Poisson's ratio to analyze the ratio of distortion to dilatation at the yield condition. During the yield condition, distortion or shape change prevails over dilatation or volume change. At fracture dilatation is at a maximum.

Literature Cited

1. Park, J. M., and Thorpe, J. L., J. of Korea TAPPI, 31(5):57 (1999).
2. Cox, H. L., Brit. J. Appl. Phys. 3(3):72-79 (1952).
3. Griffith, A. A., Philosophical transactions, Royal Society of London, Series A 221, pp. 163-198 (1921).
4. Griffith, A. A., The theory of rupture, Proceedings of First Inter'l Congress of Applied Mechanics, 1924, Biezeno & Burgers (ed.), Waltman, pp. 55-63.
5. Sih, G. C., Mechanics of Fracture Initiation and Propagation, Kluwer Academic Publishers, Dordrecht (1991).

6. Erdogen, F., Sih, G. C., J. Basic Eng., 85:519-527 (1974).
7. Sih, G. C., Int. J. Fracture, 10(3):305-321 (1974).
8. Beltrami, E., Rend. Ist. Lomb., 18:704 (1885).
9. Haigh, B. P., Brit. Ass. Reports, Section G (1919).
10. Huber, M. T., Czasopismo techniczne, Lemberg, 22:81 (1904).
11. Von Mises, R., G ttinger Nachrichten, math-phys, Klasse, pp. 582 (1913).
12. Henky, H., Zeits, ang. Math. Mech. 4:323 (1924)
13. Park, J. M., and Thorpe, J. L., J. of Korea TAPPI, 28(4):17-30 (1996).
14. Habeger, C. C., J. Eng. Mat. & Technol., 112:366-371 (1990).
15. Choi, D., Thorpe, J., Hanna, R., Wood Sci. & Tech., 25:251 (1991).
16. Kohnke, P. C. (ed.) ANSYS Engineering Analysis System, Revision 4.4. 5th ed., Houston, PA 15342, USA, Aug. 1 (1989).
17. Park, J. M., and Thorpe, J. L., J. of Korea TAPPI, 31(5):47 (1999).